Catalysis Communications 142 (2020) 106043

Contents lists available at ScienceDirect

Catalysis Communications

journal homepage: www.elsevier.com/locate/catcom

Short communication

Highly efficient and stable bicomponent cobalt oxide-copper catalysts for dehydrogenation

Yongsheng Wang[a,b], Yingying Wu[a,b], Weixiang Xu[a,b], Xinping Zhang[a,b], Tian Qiu[a,b], Shiyu Ren[c], Dongjie Guo[a,b], Li Chen[a,b], Zhengkang Duan[a,b,*]

[a] College of Chemical Engineering, Xiangtan University, Xiangtan 411105, Hunan, China
[b] Hunan Collaborative Innovation Center of New Chemical Technologies for Environmental Benignity and Efficient Resource Utilization, Xiangtan 411105, Hunan, China
[c] School of Chemistry and Chemical Engineering, South China University of Technology, Guangzhou 510641, China

ARTICLE INFO

Keywords:
Co_3O_4
Bicomponent catalyst
Strong interaction
Sintering resistant
Diethanolamine dehydrogenation

ABSTRACT

Cu/Co_3O_4-ZrO_2 catalyst was synthesized by a simple co-precipitation method, and its self-oxidation behavior after reduction reduced the particle size of Co_3O_4. Cu/Co_3O_4-ZrO_2 demonstrated a high performance during the dehydrogenation of diethanolamine, reaching a 96% yield of iminodiacetic in 30 min. The catalyst was characterized by XRD, XPS, TEM, SEM, and H_2-TPR. The results showed that strong Cu-oxide interactions, the co-catalysis of biactive components, and the higher number of oxygen vacancies of Cu/Co_3O_4-ZrO_2 were responsible for the enhanced catalytic activity during diethanolamine dehydrogenation. Co_3O_4 particles improved the dispersion and stability of Cu NPs and inhibited the sintering of loaded Cu NPs.

1. Introduction

Glyphosate is the most widely used pesticide in the world and is produced mainly from iminodiacetic acid (IDA) and glycine (Gly). The IDA method was invented by Monsanto, which currently uses it to produce glyphosate in all of its factories around the world [1]. The key reaction in an alternative, cost-efficient route for glyphosate synthesis is the dehydrogenation of diethanolamine (DEA) to form disodium iminodiacetic acid (DSIDA). Cu-based catalysts are commonly used during this reaction [2,3], but since slurry kettle-type reactions are used, the catalyst tends to lose its activity because active components easily oxidize and aggregate. During the later stages of catalyst used, the reactivity and selectivity of the catalyst typically decrease.

The development of stable and efficient catalysts is challenging, and many methods have been developed to improve the catalytic activity and anti-sintering property of Cu-based catalysts, including optimizing the preparation process of Cu NPs, selecting and pretreating carrier materials, and exploiting the constraining effect of porous channels and materials on Cu NPs [4–6]. The strategies and methods for suppressing the sintering of supported Cu NPs exploit strong metal−support interactions (SMSI) between Cu NPs and oxide supports [7]. The most effective method to improve a catalyst's activity is to increase its number of active components and active sites. Therefore, novel high-performance Cu-based catalysts can be developed by introducing new active metal oxides to construct dual-active components. Biactive components usually have higher catalytic activities than single-metal catalysts due to their synergistic catalytic effects [8]. Additionally, the introduction of new active oxides can create new environments and catalyst morphologies that can improve the catalytic performance. For example, $Ga_2O_3/Cu/ZrO_2$ catalysts can improve the selectivity of the synthesis of methanol from CO_2, increase the catalytic activity, and improve the dispersion of Cu NPs [9]. Active sites are often oxygen vacancies or coordinatively unsaturated metal cations located at the interface between Cu and oxide [10]. Therefore, the selection of active components and SMSI effects between Cu and the oxide carrier are very important for improving the activity and stability of a catalyst.

The structure and properties of nanoscale oxide carriers significantly affect the dispersion and electronic properties of Cu particles [11]. In many homogeneous catalytic reactions, ZrO_2-supported metal nanoparticles have good anti-sintering properties. As a carrier, ZrO_2 provides a charge buffer for the gain and loss of electrons of Cu. Although it is not directly involved in catalysis, it can effectively improve the activity of Cu-based catalysts [12]. As a structural stabilizer, ZrO_2 can prevent the sintering of copper NPs and prolong the service life of catalysts [13]. Co oxides are generally the most suitable alternatives to noble metal catalysts because of abundant cobalt resources and their excellent activity during catalytic oxidation [14–19]. For example, when used as a catalyst for the hydrolysis of ammonia borane to

* Corresponding author at: College of Chemical Engineering, Xiangtan University, Xiangtan 411105, Hunan, China.
E-mail address: dzk0607@163.com (Z. Duan).

https://doi.org/10.1016/j.catcom.2020.106043
Received 5 February 2020; Received in revised form 27 April 2020; Accepted 10 May 2020
Available online 11 May 2020
1566-7367/

hydrogen, Cu/Co_3O_4 showed excellent catalytic oxidation performance and could be reused 10 times without a significant loss in its catalytic performance [20]. Cu NP catalysts supported on Co_3O_4-ZrO_2 may be an ideal dual-active catalyst with an SMSI effect for the dehydrogenation of diethanolamine.

Therefore, Cu/Co_3O_4-ZrO_2 was designed and synthesized with an additional active component of Co_3O_4 to form a catalyst with two active components. Small Co_3O_4 particles were grown on the surface of ZrO_2 by reduction and self-oxidation. Moreover, irregular and fine Co_3O_4 particles confined the Cu NPs to the surface of ZrO_2. Cu/Co_3O_4-ZrO_2 showed good catalytic activity and stability when used to catalyze the dehydrogenation of diethanolamine. Cu/Co_3O_4-ZrO_2 is an excellent catalyst with controllable morphology and provides an example of a new bicomponent dehydrogenation catalyst.

2. Experimental section

2.1. Synthesis of Cu/Co_3O_4-ZrO_2

$ZrOCl_2{\cdot}8H_2O$ (6.44 g) was dissolved in 500 mL ultra-pure water, and 5 g NaOH was dissolved in 200 mL water. The NaOH solution was slowly added to the Zr salt solution and continuously stirred. After addition, the solution was stirred for 3 h to form a $Zr(OH)_2$ colloidal solution. $CoCl_6{\cdot}2H_2O$ (1.19 g) and 2.42 g $Cu(NO_3)_2{\cdot}3H_2O$ were dissolved in 200 mL ultrapure water and stirred and then slowly added to the $Zr(OH)_2$ colloidal solution and continuously stirred. After addition, the mixture was stirred for 12 h and aged for an additional 4 h. The precipitate was filtered, washed, and dried in an oven at 50 °C for 12 h. Then, the dried solid was ground and roasted in a muffle furnace at 550 °C for 4 h to obtain the catalyst precursor CuO/Co_3O_4-ZrO_2. The precursor CuO/Co_3O_4-ZrO_2 was placed into a tubular furnace and reduced at 240 °C for 4 h at a heating rate of 3 °C/min. When cooled to room temperature, the catalyst was removed from the tube furnace, and CoO was allowed to self-oxidize for 1 h to obtain Cu/Co_3O_4-ZrO_2 catalyst.

2.2. Catalytic activity evaluation

10 g Diethanolamine, 2 g catalyst, and 8.5 g sodium hydroxide (dissolved in 80 mL deionized water) were added to a high-pressure reactor. The airtightness of the reactor was checked, and then N_2 was passed and emptied 5–6 times before pressurizing to 1 MPa. The temperature was raised to 160 °C at a heating rate of 4 °C/min, and stirring was carried out at a speed of 400 rpm. The volume of hydrogen discharged was measured by a rotameter. The exhaust valve was opened when the air pressure reached 1.5 MPa and then closed when the pressure dropped to 1 MPa. The volume and exhaust temperature of each exhaust were recorded. During reactions, if the pressure in the reactor did not change for 20 min, the reaction was regarded as complete. Liquid chromatography was used for qualitative analysis. The yield of iminodiacetic acid was calculated using a strong anion exchange column (Hypersil SEX, 5 μm, 4.6 mm × 250 mm). The calculation of the yield of iminodiacetic acid is described in detail in the *Supporting Information*.

3. Results and discussion

Fig. 1 shows the XRD patterns of the catalysts. The Cu grain size in the catalyst was calculated using the Scherrer equation and the half-peak width of the highest diffraction peak of each material. Diffraction peaks of ZrO_2 were observed at 30.5°, 34.7°, 50.8°, and 60.9° (JCPDS no. 37–1484). Metallic Cu peaks appeared at 2θ values of 43.3° and 50.4°, which corresponded to the crystal planes of Cu(111) and Cu (200), respectively (JCPDS no. 04–0836). However, no metallic Cu peaks were detected in the pattern of Cu/Co_3O_4, indicating that the copper species may be amorphous and highly dispersed on the carrier

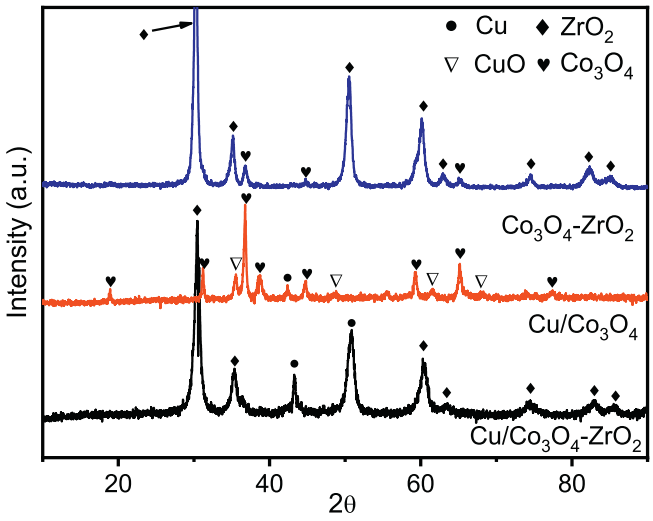

Fig. 1. XRD patterns of Cu/Co_3O_4-ZrO_2, Cu/Co_3O_4, and Co_3O_4-ZrO_2 catalysts.

[21]. The characteristic peaks of Co_3O_4 were observed at 31.3°, 36.8°, 38.5°, 44.8°, 59.5°, and 65.2° [22], which were respectively indexed to the (111), (220), (311), (222), and (400) planes. The Cu nanoparticle size in Cu/Co_3O_4-ZrO_2 was 4.7 nm as calculated from the Scherrer equation. In addition, no characteristic diffraction peaks associated with Co_3O_4 were observed for Cu/ Co_3O_4-ZrO_2, possibly because it was amorphous and highly dispersed on ZrO_2. By comparing Cu/Co_3O_4 and Co_3O_4-ZrO_2, it can be seen that a wider FWHM (full width at half maximum) of the Co_3O_4 (220) diffraction peak was observed in Co_3O_4-ZrO_2, indicating a smaller particle size. The results show that the size of Co_3O_4 was greatly reduced when Co_3O_4 was grown on the surface of ZrO_2 by reduction and self-oxidation.

Fig. 2(a) shows the SEM images of Cu/Co_3O_4-ZrO_2. The Co_3O_4 prepared by reductive self-oxidation had a small size, consistent with the XRD results. Fig. 2(b) are the TEM images of Cu/Co_3O_4-ZrO_2. According to Fig. 2(b), the diameter of Co_3O_4 was about 10 nm, and Cu and Co_3O_4 were dispersed on the surface of ZrO_2.

The H_2-TPR profiles of Cu/ZrO_2, Cu/Co_3O_4-ZrO_2, and Cu/Co_3O_4 are displayed in Fig. 3 Cu/ZrO_2 samples showed two low-temperature reduction peaks near 130 °C and 179 °C. The reduction peak at 130 °C was caused by the reduction of highly-dispersed CuO on the surface of the catalyst, while the reduction peak at 179 °C was caused by the reduction of crystalline CuO. Another reduction peak observed at 200 °C was caused by the reduction of Cu^{2+} in the ZrO_2 lattice. The two low-temperature reduction peaks of Cu/Co_3O_4-ZrO_2 samples near 126 °C and 135 °C were caused by the reduction of highly-dispersed CuO on the catalyst surface, while the reduction peaks at 162 °C were caused by the reduction of crystalline CuO. The reduction temperature stability of Cu species in Cu/Co_3O_4-ZrO_2 decreased significantly compared with Cu/ZrO_2. This indicates that the introduction of Co_3O_4 improved the dispersion of Cu NPs and that the particle size was small. The overall reduction peak temperature of Cu/Co_3O_4 Cu NPs was higher than that of Cu/Co_3O_4-ZrO_2 due to the strong interaction between Cu and the Co_3O_4 carrier. The peak at 200–260 °C was attributed to the reduction of Co^{3+} to Co^{2+} in Cu/Co_3O_4-ZrO_2 and Cu/Co_3O_4 [23]. During this process, Co_3O_4 in Cu/Co_3O_4-ZrO_2 was reduced to CoO, thus decreasing the amount of Co_3O_4. During self-oxidation, CoO self-oxidized to small Co_3O_4 particles, which grew on the surface of ZrO_2.

The influence of the surface elemental composition and chemical state on catalyst properties was studied using XPS. Fig. 4(a) shows the bimodal Co(2p) spectrum of Co_3O_4. In particular, peaks of Co $2p_{3/2}$ and $Co2p_{1/2}$ were found at 779.2–780.2 eV and 794.7–796.6 eV, respectively. The energy differences between the peak values of Co $2p_{3/2}$ and Co $2p_{1/2}$ of Cu/Co_3O_4-ZrO_2, Cu/Co_3O_4, and Co_3O_4-ZrO_2 were

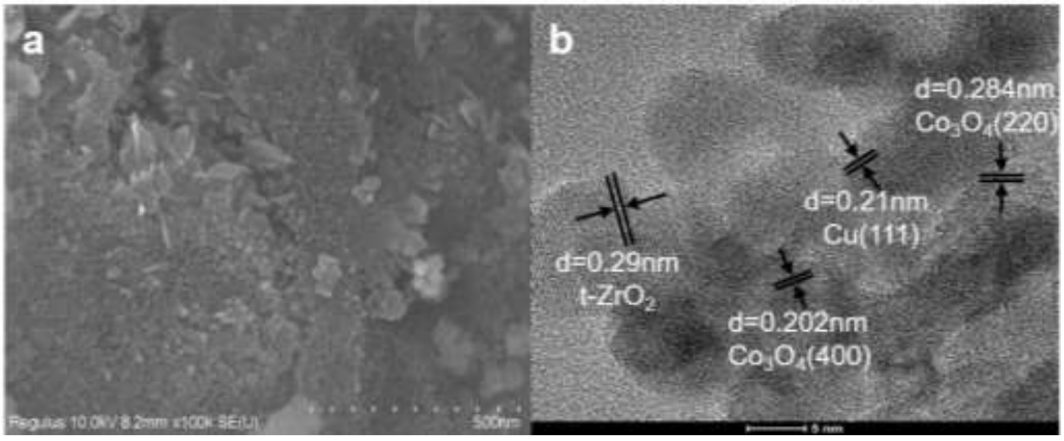

Fig. 2. The SEM images of Cu/Co_3O_4-ZrO_2 (a); TEM images of Cu/Co_3O_4-ZrO_2 (b).

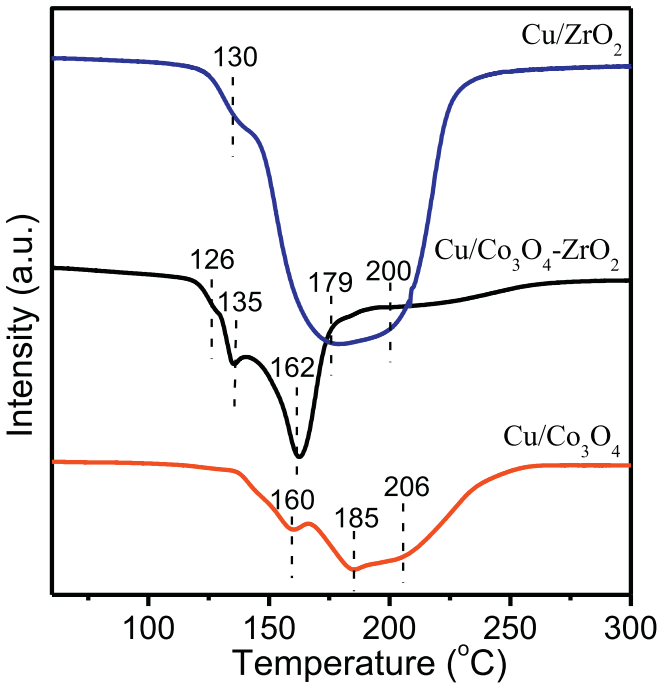

Fig. 3. H_2-TPR patterns of the catalysts.

respectively 16.4, 15.6, and 15 eV, indicating the existence of Co_3O_4 [24]. The XPS peaks of Cu 2p were observed at 933.1/933.4 eV and 953.0/953.6 eV with strong shake-up satellite peaks in the patterns of Cu/Co_3O_4-ZrO_2 and Cu/Co_3O_4. The satellite peaks indicated that the Cu species in Cu/Co_3O_4-ZrO_2 and Cu/Co_3O_4 was Cu(II) [25] (Fig. S1). Fig. 4(b) shows the deconvolution peaks of O of Cu/Co_3O_4-ZrO_2, Cu/Co_3O_4, and Cu/ZrO_2 samples. The patterns of all three samples contained diffraction peaks near 529.8 eV and 531.5 eV, which respectively corresponded to lattice O and defect oxygen vacancies (dissociated adsorptive oxygen). By integrating the spectrum of Cu/Co_3O_4-ZrO_2, oxygen vacancies were determined to account for 29.4%, 28.0%, and 15.0% of all O present in Cu/Co_3O_4 and Cu/ZrO_2, respectively. Co_3O_4 may have grown on the surface of ZrO_2 to produce highly-active defective oxygen vacancies. The oxygen vacancies content of Cu/Co_3O_4-ZrO_2 was the highest, leading to its excellent catalytic activity, which was conducive to the rapid dehydrogenation of diethanolamine.

The catalysts were used in the dehydrogenation of diethanolamine to prepare iminodiacetic acid. The catalytic activity performance results are shown in Table 1. Cu/Co_3O_4-ZrO_2 had the highest activity and fastest reaction time compared with literature and commercial catalysts. This was caused by Cu and Co_3O_4 co-catalysis and the additional oxygen vacancies which can quickly absorb diethanolamine. Cu and Co_3O_4 promoted catalysis by forming an aldehyde intermediate by α-H cleavage. Second, the introduction of Co_3O_4 increased the density of active sites which helped form surface oxygen vacancies by improving the adsorption-activation of reactant molecules over active sites due to strong metal-oxide interactions. The abundant oxygen vacancies and Co_3O_4 species dramatically enhanced the oxidation of hydroxyls to

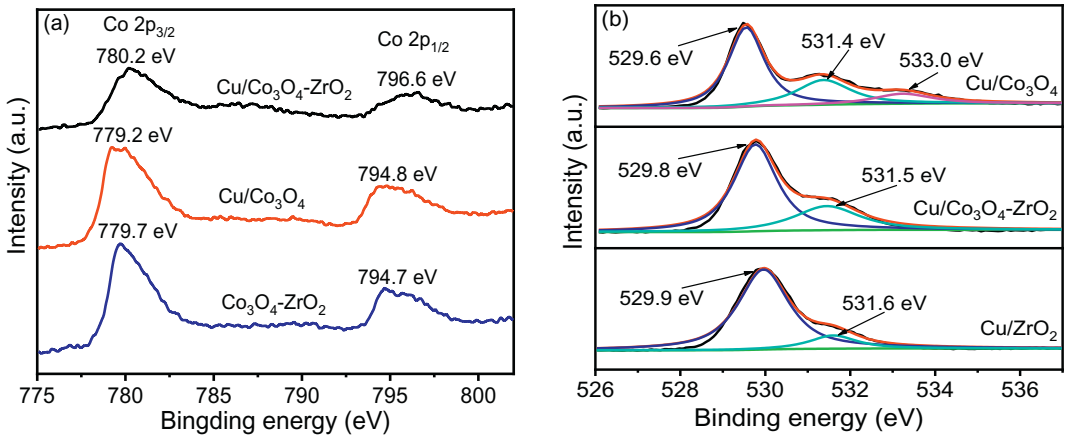

Fig. 4. XPS spectra of Co 2p (a) and O (b).

Table 1
Activity test results of samples in the dehydrogenation of diethanolamine.

Catalyst	IDA Yield (%)	Reaction time/ min	Reaction temperature/ °C
Cu/ZrO_2	92	150	160
Cu/Co_3O_4-ZrO_2	96	30	160
Cycle 2 of Cu/Co_3O_4-ZrO_2	95	32	160
Cu/Co_3O_4	90	240	160
Co_3O_4-ZrO_2	60	480	170
CZ@CN[2]	92	90	160
Cu/ZrO_2-RGO[3]	90	75	160
Raney Cu	98	600	160
ZrO_2	0	600	160

aldehyde intermediates. In addition, the much larger surface area of Cu/Co_3O_4-ZrO_2 (61 m^2/g) than Cu/ ZrO_2 (23 m^2/g) was possibly due to the addition of transition metals, which were 11.1% (Cu) and 5.8% (Co) (Table S1). Therefore, the Cu/Co_3O_4-ZrO_2 catalyst showed excellent catalytic performance, and a 96% yield of IDA was achieved within 30 min.

To determine whether Co_3O_4 had a catalytic oxidation effect on diethanolamine, Co_3O_4 was loaded onto ZrO_2 to prepare a Co_3O_4-ZrO_2 catalyst. A yield of 60% was obtained after a 480 min reaction. Since ZrO_2 had no catalytic effect on the reaction, it was determined that Co_3O_4 was responsible for the catalytic oxidation during the reaction. Compared with Cu/ZrO_2-RGO catalysts in the literature, the reaction time decreased by 60% from 75 min to 30 min.

TEM, XRD, and XPS were used to characterize catalysts after the reactions to explore the state of the active species after a reaction. Fig. S2(b) shows that Co_3O_4 contained small particles on the surface of ZrO_2 before and after the reaction. The particle size was 10 nm after the reaction, which was the same as the fresh catalyst. Fig. S2(d) shows XRD patterns of fresh and used Cu/Co_3O_4-ZrO_2 catalysts. Compared with the fresh catalyst, the position and strength of the Cu/Co_3O_4-ZrO_2 diffraction peak did not significantly change after the reaction, indicating that Cu/Co_3O_4-ZrO_2 was stable because strong interactions between the metal prevented agglomeration during sintering. Fig. S2(e, f) shows the deconvoluted Co $2p_{3/2}$ peaks of fresh and post-reaction catalyst. The intensity of the peaks at 781.3 eV and 786.3 eV increased after the reaction, indicating that $Co(OH)_2$ was formed on the catalyst surface after the reaction [26,27].

4. Conclusions

A CuO/Co_3O_4-ZrO_2 precursor was obtained by co-precipitation, and a bicomponent Cu/Co_3O_4-ZrO_2 catalyst was successfully prepared by reduction and self-oxidation. When used in the dehydrogenation of diethanolamine to prepare IDA, the Cu/Co_3O_4-ZrO_2 catalyst showed excellent catalytic performance, and a 96% yield of IDA was achieved within 30 min. The inclusion of a biactive component was key to increasing the catalytic activity of Cu/Co_3O_4-ZrO_2 catalysts during diethanolamine dehydrogenation. It was also important to include Co_3O_4 to increase the number of oxygen vacancy defects in the catalyst during the catalytic dehydrogenation of diethanolamine. The strong interactions between metal (Cu) and oxide (Co_3O_4-ZrO_2) helped improve the stability and activity of the catalyst. The results of this study suggest that Co_3O_4 can be used as an active component to enhance the performances of Cu-based nanocatalysts, and this work provides a new strategy for developing other advanced dehydrogenation catalysts.

Declaration of Competing Interest

The authors declare that they have no known competing financial interests or personal relationships that could have appeared to influence the work reported in this paper.

Acknowledgment

This work was supported by the National Natural Science Foundation of China (21576229).

Appendix A. Supplementary data

Supplementary data to this article can be found online at https://doi.org/10.1016/j.catcom.2020.106043.

References

[1] D.A. Hickman, K. Mosner, J.W. Ringer, A continuous diethanolamine dehydrogenation fixed bed catalyst and reactor system, Chem. Eng. J. 278 (2015) 447–453.
[2] Y. Wang, Y. Zhao, Z. Zhao, X. Lan, J. Xu, W. Xu, Z. Duan, Study on preparation of cu-ZrO_2 catalyst coated by nitrogen-doped carbon and catalytic dehydrogenation performance, Acta Chim. Sin. 77 (2019) 661–668.
[3] Y. Wang, Z. Zhao, Y. Zhao, X. Lan, W. Xu, L. Chen, D. Guo, Z. Duan, A ZrO_2-RGO composite as a support enhanced the performance of a Cu-based catalyst in dehydrogenation of diethanolamine, RSC Adv. 9 (2019) 30439–30447.
[4] J. Yuan, S.S. Li, L. Yu, Y.M. Liu, Y. Cao, H.Y. He, K.N. Fan, Copper-based catalysts for the efficient conversion of carbohydrate biomass into γ-valerolactone in the absence of externally added hydrogen, Energy Environ. Sci. 6 (2013) 3308–3313.
[5] X. Lan, Z. Duan, Y. Wang, J. Xu, Advance in synthesizing Cu-based catalysts applying to dehydrogenation process, Pet. Chem. 59 (2019) 1169–1176.
[6] M. Gawande, A. Goswami, F. Felpin, T. Asefa, X. Huang, R. Silva, X. Zou, R. Zboril, R. Varma, Cu and cu-based nanoparticles: synthesis and applications in catalysis, Chem. Rev. 116 (2016) 3722–3811.
[7] J. Li, Q. Guan, H. Wu, W. Liu, Y. Lin, Z. Sun, X. Ye, X. Zheng, H. Pan, J. Zhu, S. Chen, W. Zhang, S. Wei, J. Lu, Highly active and stable metal single-atom catalysts achieved by strong electronic metal-support interactions, J. Am. Chem. Soc. 141 (2019) 14515–14519.
[8] J. Zhang, Z. Gao, S. Wang, G. Wang, X. Gao, B. Zhang, S. Xing, S. Zhao, Y. Qin, Origin of synergistic effects in bicomponent cobalt oxide-platinum catalysts for selective hydrogenation reaction, Nat. Commun. 10 (2019) 4166–4176.
[9] E.L. Fornero, A.L. Bonivardi, M.A. Baltanás, Isotopic study of the rates of hydrogen provision vs. methanol synthesis from CO_2 over Cu-Ga-Zr catalysts, J. Catal. 330 (2015) 302–310.
[10] Z. Liu, Z. Wu, X. Peng, A. Binder, S. Chai, S. Dai, Origin of active oxygen in a ternary CuO_x/Co_3O_4-CeO_2 catalyst for CO oxidation, J. Phys. Chem. C 118 (2014) 27870–27877.
[11] Y.F. Zhu, X. Kong, X. Li, G. Ding, Y. Zhu, Y.W. Li, Cu nanoparticles inlaid mesoporous Al_2O_3 as a high-performance bifunctional catalyst for ethanol synthesis via dimethyl oxalate hydrogenation, ACS Catal. 4 (2014) 3612–3620.
[12] Q.L. Tang, Z.P. Liu, Identification of the active cu phase in the water-gas shift reaction over Cu/ZrO_2 from first principles, J. Phys. Chem. C 114 (2010) 8423–8430.
[13] J. Agrell, Production of hydrogen from methanol over Cu/ZnO catalysts promoted by ZrO_2 and Al_2O_3, J. Catal. 219 (2003) 389–403.
[14] S. Gao, Y. Lin, X. Jiao, Y. Sun, Q. Luo, W. Zhang, D. Li, J. Yang, Y. Xie, Partially oxidized atomic cobalt layers for carbon dioxide electroreduction to liquid fuel, Nature 529 (2016) 68–71.
[15] A. Jha, C.V. Rode, Highly selective liquid-phase aerobic oxidation of vanillyl alcohol to vanillin on cobalt oxide nanoparticles, New J. Chem. 39 (2013) 2669–2674.
[16] X. Xie, Y. Li, Z. Liu, M. Haruta, W. Shen, Low-temperature oxidation of CO catalyzed by Co_3O_4 nanorods, Nature 458 (2009) 746–749.
[17] Y. Zheng, Y. Liu, H. Zhou, W. Huang, Z. Pu, Complete combustion of methane over Co_3O_4 catalysts: influence of pH values, J. Alloys Compd. 734 (2018) 112–120.
[18] W. Tang, W. Xiao, S. Wang, Z. Ren, J. Ding, P.X. Gao, Boosting catalytic propane oxidation over PGM-free Co_3O_4 nanocrystal aggregates through chemical leaching: a comparative study with Pt and Pd based catalysts, Appl. Catal. B Environ. 226 (2018) 585–595.
[19] G. Li, C. Zhang, Z. Wang, H. Huang, H. Peng, X. Li, Fabrication of mesoporous Co_3O_4 oxides by acid treatment and their catalytic performances for toluene oxidation, Appl. Catal. A Gen. 550 (2018) 67–76.
[20] Y. Yamada, K. Yano, Q. Xu, S. Fukuzumi, Cu/Co_3O_4 nanoparticles as catalysts for hydrogen evolution from ammonia borane by hydrolysis, J. Phys. Chem. C 114 (2010) 16456–16462.
[21] M.F. Luo, Y.P. Song, J.Q. Lu, X.Y. Wang, Z.Y. Pu, Identification of CuO species in high surface area CuO-CeO_2 catalysts and their catalytic activities for CO oxidation, J. Phys. Chem. C 111 (2007) 12686–12692.
[22] H. Wang, H. Zhu, Z. Qin, F. Liang, G. Wang, J. Wang, Deactivation of a au/CeO_2-Co_3O_4 catalyst during CO preferential oxidation in H_2-rich stream, J. Catal. 264 (2009) 154–162.
[23] L. Lukashuk, K. Föttinger, E. Kolar, C. Rameshan, D. Teschner, M. Hävecker, A. Knop-Gericke, N. Yigit, H. Li, E. McDermott, M. Stöger-Pollach, G. Rupprechter, Operando XAS and NAP-XPS studies of preferential CO oxidation on Co_3O_4 and CeO_2-Co_3O_4 catalysts, J. Catal. 344 (2016) 1–15.

[24] K. Yin, J. Ji, Y. Shen, Y. Xiong, H. Bi, J. Sun, T. Xu, Z. Zhu, L. Sun, Magnetic properties of Co_3O_4 nanoparticles on graphene substrate, J. Alloys Compd. 720 (2017) 345–351.
[25] Y. Wang, H. Zhu, Z. Duan, Z. Zhao, Y. Zhao, X. Lan, L. Chen, D. Guo, Study on the structure of cu/ZrO_2 catalyst and the formation mechanism of disodium imino-diacetate and sodium glycine, Catal. Lett. 150 (2020) 1111–1120.
[26] J. Yang, H. Liu, W.N. Martens, R.L. Frost, Synthesis and characterization of cobalt hydroxide, cobalt oxyhydroxide, and cobalt oxide nanodiscs, J. Phys. Chem. C 114 (2010) 111–119.
[27] T. Mathew, N.R. Shiju, K. Sreekumar, B.S. Rao, C.S. Gopinath, Cu-Co synergism in $Cu_{1-x}Co_xFe_2O_4$ -catalysis and XPS aspects, J. Catal. 210 (2002) 405–417.